DPCore: Dynamic Prompt Coreset for Continual Test-Time Adaptation

Yunbei Zhang [1] **Akshay Mehra** [1] **Shuaicheng Niu** [2] **Jihun Hamm** [1]

Abstract

Continual Test-Time Adaptation (CTTA) faces challenges when real-world domains are dynamic—recurring with varying frequencies and durations—unlike the structured changes many methods assume. Existing approaches then struggle with convergence issues from brief domain exposures, catastrophic forgetting, and knowledge misapplication in these dynamic conditions. We propose **DPCore**, a robust and computationally efficient method designed for such dynamic patterns. DPCore integrates three key components: Visual Prompt Adaptation for efficient domain alignment, a Prompt Coreset for knowledge preservation, and a Dynamic Update mechanism that intelligently manages prompts based on domain similarity. Extensive experiments on four benchmarks show DPCore achieves state-of-the-art performance in both structured and dynamic settings, significantly reducing trainable parameters by 99% and computation time by 64% compared to previous approaches.

1. Introduction

Deep Neural Networks often suffer performance degradation when facing domain discrepancies between training and test environments (Recht et al., 2019; Hendrycks & Dietterich, 2019; Koh et al., 2021). Test-Time Adaptation (TTA) (Wang et al., 2021; Xiao & Snoek, 2024; Liang et al., 2020) adapts pre-trained models to unseen target domains without altering the original training process.

Real-world scenarios present an even more challenging problem: continuously changing target domains. While Continual Test-Time Adaptation (CTTA) (Wang et al., 2022; Niu et al., 2022) has emerged to address this challenge, the initial CTTA setting (Wang et al., 2022), which we term Continual Structured Change (**CSC**), assumed domains change

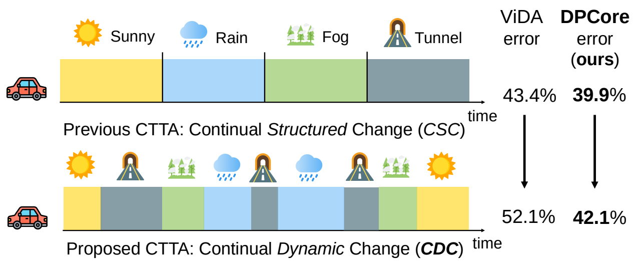
Sunny
Rain
Fog
Tunnel
ViDA error
DPCore error (ours)
43.4%
39.9%
time
Previous CTTA: Continual *Structured* Change (*CSC*)
52.1%
42.1%
time
Proposed CTTA: Continual *Dynamic* Change (*CDC*)

Figure 1. Illustrated through an autonomous driving scenario where a vehicle encounters varying weather and lighting conditions. The top panel shows the conventional CSC setting with structured, uniform-length domain transitions, while the bottom panel illustrates our proposed CDC setting where domains recur with varying frequencies and durations—better reflecting real-world challenges. When evaluated on ImageNet-to-ImageNet-C with ViT base model, previous SOTA ViDA's error rate increases significantly from 43.4% to 52.1% when moving from CSC to CDC, while DPCore maintains robust performance (39.9% to 42.1%).

with uniform durations. However, real-world scenarios exhibit far more dynamic patterns where domains recur with varying frequencies and durations, which we term Continual Dynamic Change (**CDC**). For instance, an autonomous vehicle driving through mountains frequently transitions between sunny conditions, dark tunnels, fog, and rain, as illustrated in Fig. 1. Our experiments show state-of-the-art (SOTA) methods like ViDA (Liu et al., 2023b) suffer substantial degradation, with error rates increasing by 8.7% on ImageNet-to-ImageNet-C when moving from CSC to CDC.

In CDC, existing CTTA methods face three critical limitations: *Convergence Issues* when domains appear briefly, *Catastrophic Forgetting* as knowledge from previous domains is overwritten, and *Negative Transfer* when knowledge from one domain adversely affects adaptation to different domains (Fig. 4b). Furthermore, current approaches are computationally intensive, requiring extensive data augmentation (Wang et al., 2022; Liu et al., 2023b) or numerous additional parameters with pre-adaptation warm-up (Liu et al., 2023b; Song et al., 2023; Gan et al., 2023).

To address these challenges, we introduce **D**ynamic **P**rompt **Core**set (**DPCore**), a novel CTTA method for robust performance across varying domain change patterns while maintaining computational efficiency. As shown in Fig. 2, DPCore combines: (1) *Visual Prompt Adaptation* (VPA) that

[1]Tulane University [2]Nanyang Technological University. Correspondence to: Yunbei Zhang <yzhang111@tulane.edu>, Jihun Hamm <jhamm3@tulane.edu>.

ICML 2025 Workshop on Test-Time Adaptation: Putting Updates to the Test.

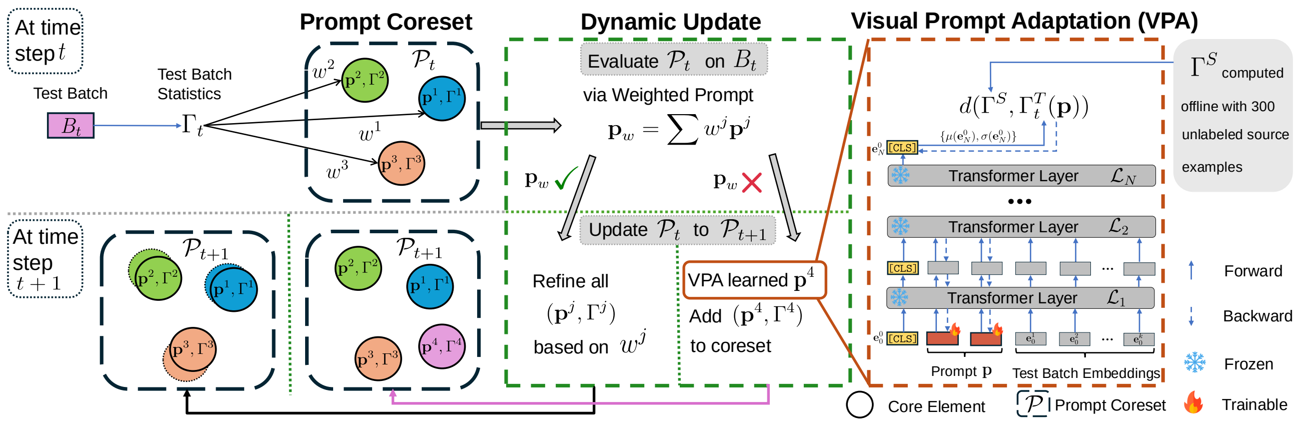
At time step t
Test Batch
B_t
Test Batch Statistics
Γ_t
Prompt Coreset
$\mathcal{P}_t$
w^1
w^2
w^3
$\mathbf{p}^1, \Gamma^1$
$\mathbf{p}^2, \Gamma^2$
$\mathbf{p}^3, \Gamma^3$
Dynamic Update
Evaluate $\mathcal{P}_t$ on B_t
via Weighted Prompt
$\mathbf{p}_w = \sum w^j \mathbf{p}^j$
$\mathbf{p}_w$ ✓
$\mathbf{p}_w$ ✗
Update $\mathcal{P}_t$ to $\mathcal{P}_{t+1}$
Refine all $(\mathbf{p}^j, \Gamma^j)$ based on w^j
VPA learned $\mathbf{p}^4$
Add $(\mathbf{p}^4, \Gamma^4)$ to coreset
At time step $t+1$
$\mathcal{P}_{t+1}$
$\mathbf{p}^4, \Gamma^4$
Visual Prompt Adaptation (VPA)
$d(\Gamma^S, \Gamma^T_t(\mathbf{p}))$
$\{\mu(\mathbf{e}^0_N), \sigma(\mathbf{e}^0_N)\}$
Γ^S computed offline with 300 unlabeled source examples
Transformer Layer $\mathcal{L}_N$
Transformer Layer $\mathcal{L}_2$
Transformer Layer $\mathcal{L}_1$
[CLS]
Prompt $\mathbf{p}$
Test Batch Embeddings
Forward
Backward
Frozen
Trainable
Core Element
Prompt Coreset

Figure 2. Overview of DPCore. At time step t, Prompt Coreset $\mathcal{P}_t$ (upper left) maintains core elements consisting of learned prompts $\boldsymbol{p}^j$ and statistics Γ^j from previous domains. Dynamic Update (middle) evaluates new test batch B_t by computing a weighted prompt $\boldsymbol{p}_w$ based on distances between batch statistics Γ_t and core elements Γ^j. If $\boldsymbol{p}_w$ performs well, existing core elements $\{\boldsymbol{p}^j, \Gamma^j\}$ are refined using weights w^j; otherwise, VPA (right) learns a new prompt by aligning the test batch with source statistics (computed offline from 300 examples) and adds it to the prompt coreset. The updated coreset $\mathcal{P}_{t+1}$ is then used for the next time step $t+1$.

aligns domains with minimal parameters and no warm-up, (2) a *Prompt Coreset* that preserves knowledge from previous domains, and (3) a *Dynamic Update* mechanism that adjusts prompts based on domain similarities. DPCore requires only negligible parameters and merely 300 unlabeled source examples, eliminating expensive warm-up procedures (see Table 10 and Fig. 6c).

Our experiments across four CTTA benchmarks demonstrate DPCore's superiority. On ImageNet-to-ImageNet-C, DPCore achieves +15.9% improvement over the source model in CSC, and maintains robust performance in CDC with a 42.1% error rate, outperforming ViDA by 10.0%. Our contributions are: (1) We introduce Continual Dynamic Change (CDC), a new CTTA setup that better reflects real-world scenarios through frequent domain shifts and varying durations; (2) We propose DPCore, a dynamic CTTA approach that effectively manages domain knowledge through a dynamic prompt coreset; (3) We show that DPCore is theoretically sound and achieves SOTA results for classification and segmentation tasks in both settings while being computationally efficient.

2. Preliminaries and Problem Formulation

In this section, we introduce Vision Transformers (ViTs) and define the CTTA problem across both CSC and our proposed CDC settings. Due to page limits, **detailed discussions on related work are provided in Appendix A.**

Vision Transformers (ViTs). We focus on Vision Transformers for their strong representation capabilities (Dosovitskiy et al., 2021; Liu et al., 2021). A ViT f with N transformer layers comprises a feature extractor $\phi : \mathcal{X} \to \mathcal{Z}$ (parameter θ_ϕ) and a classifier $h : \mathcal{Z} \to \mathcal{Y}$ (parameter θ_h), so $f = h \circ \phi$. Let $\boldsymbol{E}_i = \{\boldsymbol{e}_i^j\}_{j=0}^k$ be the input sequence to the $(i+1)$-th layer, where k is the number of patches and $\boldsymbol{e}_i^0$ is the classification token from layer $\mathcal{L}_i$:

$$\boldsymbol{E}_i = \phi(\boldsymbol{E}_{i-1}),\ i = 1, ..., N \quad (1)$$

$$\hat{y} = h(\boldsymbol{e}_N^0) \quad (2)$$

Continual Dynamic Change: A new CTTA setup. Given a model f_θ pre-trained on source domain $\mathcal{D}^S = (X^S, Y^S)$, CTTA adapts this model to a sequence of unlabeled target domains $\{\mathcal{D}^{T_1}, \mathcal{D}^{T_2}, ..., \mathcal{D}^{T_M}\}$. The model processes test batches $\{B_t\}_{t=1}^\infty$ sequentially, with all samples in batch B_t assumed to belong to the same unknown target domain (Wang et al., 2022; Yang et al., 2024). At each step t, parameters update from θ_t to θ_{t+1} using B_t to enhance future performance. Previous CTTA settings (Wang et al., 2022; Liu et al., 2023b; 2024) typically assume Continual Structured Change (CSC), where domains change with uniform length at regular intervals (Fig. 1 Top). However, real-world scenarios exhibit more dynamic patterns where domains recur with varying durations (Fig. 1 Bottom), which we term Continual Dynamic Change (CDC). We simulate this using a Dirichlet distribution with parameter δ: smaller δ values create transitions closer to CSC, while larger values produce more frequent and unpredictable domain changes (Fig. 4a). We set $\delta = 1$ for our main experiments to balance structured and random changes. Various δ values and other distributions are discussed in Appendix E.

3. Dynamic Prompt Coreset (DPCore)

Visual Prompt Adaptation (VPA). We leverage visual prompts (Jia et al., 2022; Ge et al., 2023) by introducing L learnable tokens $\boldsymbol{p} := \{\texttt{[Prompt]}_i\}_{i=1}^L$, where $\texttt{[Prompt]} \in \mathbb{R}^{768}$ for ViT-Base. These prompts augment the input sequence as $\boldsymbol{E}_i' = \{\boldsymbol{e}_i^0, \boldsymbol{p}, \boldsymbol{e}_i^1, ..., \boldsymbol{e}_i^k\}$, modifying

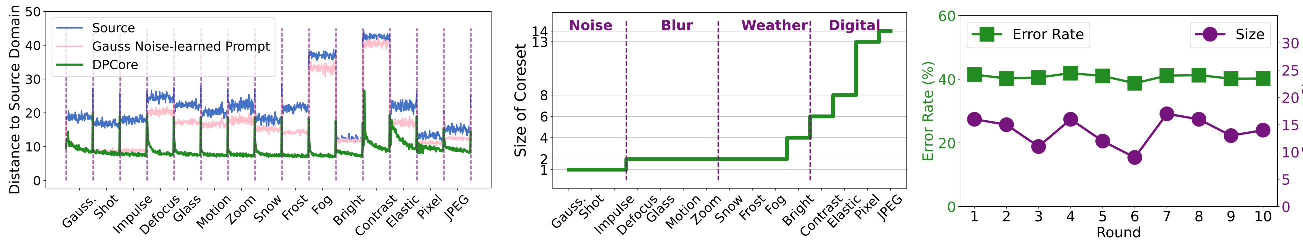

(a) Distance (b) Growth of Coreset (c) Ten Different Orders

Figure 3. Analysis of DPCore on ImageNet-to-ImageNet-C in the CSC setting. (a) Distance between test batches and source domain in Eq. (3) using source model (baseline), DPCore, and a prompt trained only on Gaussian Noise. DPCore consistently reduces domain gaps across all corruptions. (b) Evolution of coreset size across corruption types, showing strategic grouping within the four main corruption categories (Noise, Blur, Weather, Digital). (c) Performance stability across ten different domain orders.

Eq. (1) to: $\boldsymbol{E}'_i = \phi(\boldsymbol{E}'_{i-1}), \ \forall\, i = 1, ..., N$. We first extract source features $\mathcal{Z}^S = \phi(\mathcal{X}^S; \theta_\phi)$ before adaptation. For batch B_t^T at time t, we initialize prompt tokens from a Gaussian distribution without warm-up and denote extracted features with prompt $\boldsymbol{p}$ as $\mathcal{Z}_t^T(\boldsymbol{p}) := \phi(B_t^T; \theta_\phi, \boldsymbol{p})$. We align statistics (mean and standard deviation) of B_t^T, $\Gamma_t^T(\boldsymbol{p}) := \{\boldsymbol{\mu}_t^T(\boldsymbol{p}), \boldsymbol{\sigma}_t^T(\boldsymbol{p})\}$ with source $\Gamma^S := \{\boldsymbol{\mu}^S, \boldsymbol{\sigma}^S\}$ through:

$$d(\Gamma^S, \Gamma_t^T(\boldsymbol{p})) = \|\boldsymbol{\mu}^S - \boldsymbol{\mu}_t^T(\boldsymbol{p})\|_2 + \|\boldsymbol{\sigma}^S - \boldsymbol{\sigma}_t^T(\boldsymbol{p})\|_2 \tag{3}$$

The prompt is learned by minimizing this distance:

$$\boldsymbol{p}^* = \arg\min_{\boldsymbol{p}} \ d(\Gamma^S, \Gamma_t(\boldsymbol{p})) \tag{4}$$

where we omit superscript T for simplicity.

Prompt Coreset. To address catastrophic forgetting (Niu et al., 2022; Kirkpatrick et al., 2017), we introduce a Prompt Coreset mechanism inspired by Online K-Means (Duda & Hart, 1973). The coreset starts empty and updates at each time step: $\mathcal{P}_t \to \mathcal{P}_{t+1}$. Each core element contains a learned prompt and its feature statistics. When the first batch B_1 arrives, we extract features without prompt ($\mathcal{Z}_1$), compute statistics $\Gamma_1 = \{\boldsymbol{\mu}_1, \boldsymbol{\sigma}_1\}$, learn a prompt $\boldsymbol{p}_1$, and store the pair $(\boldsymbol{p}_1, \Gamma_1)$ in the coreset.

Dynamic Update to the Prompt Coreset. Our studies show prompts from one domain can benefit adaptation to similar domains but may harm performance on different domains (Appendix Table 3). Based on this, we first evaluate $\mathcal{P}_t$ on B_t via Weighted Prompt. For time step $t > 1$ with K coreset elements $\{(\boldsymbol{p}^j, \Gamma^j)\}_{j=1}^K$, we extract features $\mathcal{Z}_t$ without prompt and compute statistics Γ_t. We then generate a weighted prompt $\boldsymbol{p}_w$ as:

$$\boldsymbol{p}_w := \sum_{j=1}^{K} w^j \boldsymbol{p}^j, \qquad \text{where} \ \ w^j = \frac{\exp(-d(\Gamma_t, \Gamma^j)/\tau)}{\sum_{l=1}^{K} \exp(-d(\Gamma_t, \Gamma^l)/\tau)} \tag{5}$$

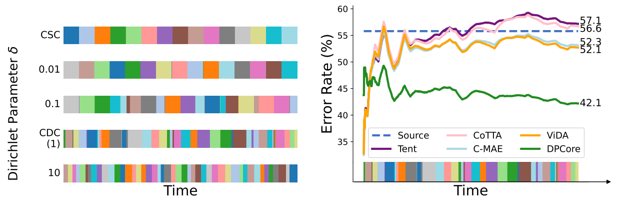

(a) Different δ (b) Error Rate in CDC

Figure 4. Analysis of CDC setting on ImageNet-to-ImageNet-C. (a) Domain change patterns with varying Dirichlet distribution parameter δ (colors represent different domains): smaller δ produces CSC-like structured changes while larger δ leads to more frequent and unpredictable transitions. (b) Performance comparison in CDC setting ($\delta = 1$), where previous methods show significant degradation while DPCore maintains robust performance.

where τ is a temperature parameter. This approach allows flexible adaptation when a domain shares characteristics with multiple visited domains. Subsequently, we update $\mathcal{P}_t$ to $\mathcal{P}_{t+1}$. We evaluate $\boldsymbol{p}_w$ by comparing distances $d(\Gamma^S, \Gamma_t)$ and $d(\Gamma^S, \Gamma_t(\boldsymbol{p}_w))$. If reduction is insufficient (potential new domain), we learn a new prompt and add it to the coreset. Otherwise, we refine $\boldsymbol{p}_w$ and update core elements:

$$\boldsymbol{p}^j \leftarrow \boldsymbol{p}^j + \alpha w^j(\boldsymbol{p}_t - \boldsymbol{p}^j), \ \Gamma^j \leftarrow \Gamma^j + \alpha w^j(\Gamma_t - \Gamma^j). \tag{6}$$

We use the ratio $\frac{d(\Gamma^S, \Gamma_t(\boldsymbol{p}_w))}{d(\Gamma^S, \Gamma_t)}$ compared to threshold ρ to determine domain novelty, allowing dynamic coreset growth based on domain complexity (Fig. 3b).

Analysis Under the assumption of well-separated domain clusters, we prove DPCore: 1) correctly assigns batches to clusters regardless of sequence length, 2) maintains correct assignments regardless of batch order, and 3) produces order-independent learned prompts. These properties enable effective domain knowledge management in dynamic environments. Details in Appendix C.4.

Table 1. Classification error rate (%) for ImageNet-to-ImageNet-C in previous CSC setting, evaluated on ViT-Base with corruption severity level 5. **Bold** and $\underline{\text{underline}}$ indicate best and second-best performance respectively.

Algorithm	Gauss.	Shot	Impulse	Defocus	Glass	Motion	Zoom	Snow	Frost	Fog	Bright	Contrast	Elastic	Pixel	JPEG	Mean↓	Gain↑
Source	53.0	51.8	52.1	68.5	78.8	58.5	63.3	49.9	54.2	57.7	26.4	91.4	57.5	38.0	36.2	55.8	0.0
Pseudo (Lee, 2013)	45.2	40.4	41.6	51.3	53.9	45.6	47.7	40.4	45.7	93.8	98.5	99.9	99.9	98.9	99.6	61.2	-5.4
Tent (Wang et al., 2022)	52.2	48.9	49.2	65.8	73.0	54.5	58.4	44.0	47.7	50.3	23.9	72.8	55.7	34.4	33.9	51.0	+4.8
CoTTA (Wang et al., 2022)	52.9	51.6	51.4	68.3	78.1	57.1	62.0	48.2	52.7	55.3	25.9	90.0	56.4	36.4	35.2	54.8	+1.0
VDP (Gan et al., 2023)	52.7	51.6	50.1	58.1	70.2	56.1	58.1	42.1	46.1	45.8	23.6	70.4	54.9	34.5	36.1	50.0	+5.8
SAR (Niu et al., 2023)	$\underline{45.8}$	45.9	47.7	52.3	63.7	46.2	50.9	40.3	42.4	41.8	24.4	53.4	53.6	38.4	36.6	45.6	+10.2
RoTTA (Yuan et al., 2023)	51.5	50.3	51.7	60.4	58.7	52.6	54.8	47.2	43.5	42.8	25.9	49.1	48.8	46.3	39.7	48.2	+7.6
EcoTTA (Song et al., 2023)	48.1	45.6	46.3	56.5	67.1	50.4	57.1	41.3	44.5	43.8	24.1	71.6	54.8	34.1	34.8	48.0	+7.8
ViDA (Liu et al., 2023b)	47.7	42.5	42.9	52.2	56.9	45.5	48.9	38.9	42.7	40.7	24.3	$\underline{52.8}$	49.1	33.5	33.1	43.4	+12.4
BGD (Yang et al., 2024)	47.5	42.1	$\underline{41.6}$	55.5	55.4	$\underline{44.5}$	47.9	$\underline{38.8}$	37.8	$\underline{39.6}$	23.6	57.0	44.4	33.5	32.3	42.8	+13.0
C-MAE (Liu et al., 2024)	46.3	$\underline{41.9}$	42.5	$\underline{51.4}$	$\underline{54.9}$	**43.3**	**40.7**	**34.2**	**35.8**	64.3	$\underline{23.4}$	60.3	**37.5**	**29.2**	$\underline{31.4}$	$\underline{42.5}$	$\underline{+13.3}$
DPCore (Proposed)	**42.2**	**38.7**	**39.3**	**47.2**	**51.4**	47.7	$\underline{46.9}$	39.3	$\underline{36.9}$	**37.4**	**22.0**	**44.4**	$\underline{45.1}$	$\underline{30.9}$	**29.6**	**39.9**	**+15.9**

4. Experiments

Experimental Setup We evaluate on three classification datasets (ImageNet-to-ImageNet-C (I2I-C), CIFAR100/10-to-CIFAR100/10C) with 15 corruption types at severity level 5, and a segmentation dataset (Cityscapes-ACDC). We compare against strong CTTA baselines including Tent (Wang et al., 2021), CoTTA (Wang et al., 2022), ViDA (Liu et al., 2023b), and C-MAE (Liu et al., 2024). We test in both CSC setting following (Wang et al., 2022) and our proposed CDC setting using Dirichlet distribution with $\delta = 1$. Implementation details, including hyperparameter selection and model configurations, are available in Appendix B and C.3.

Main Results. We present results on I2I-C across both settings, with CIFAR10/100 and Cityscapes-to-ACDC results in Appendix D.3. In the CSC setting (Table 1), DPCore achieves a SOTA improvement of +15.9% over the source model, surpassing C-MAE by 2.6%. DPCore groups similar corruptions (e.g., entire Noise group with a single core element) while learning separate elements for significantly different domains, maintaining efficiency with just 14 core elements total. It shows consistent performance across 10 random domain orders, averaging 40.2% error rate with 13.9 elements (Fig. 3c). In the more challenging CDC setting (Fig. 4b), existing methods suffer severe degradation (ViDA: 43.4% $\rightarrow$ 52.1%, Tent: 51.0% $\rightarrow$ 57.1%), while DPCore shows remarkable resilience with only a modest increase (39.9% $\rightarrow$ 42.1%), outperforming others by 10.0%. DPCore adapts by increasing its coreset from 14 to 25 elements, enabling stability across diverse scenarios.

Ablation Studies. We conduct comprehensive ablation studies on I2I-C in the CSC setting. Table 2 demonstrates the contribution of each component: using only Visual Prompt Adaptation (VPA) with Dynamic Update (DU) yields a 4.8% improvement, adding Prompt Coreset (PC) without DU increases to 7.5%, and replacing VPA with NormLayer parameters still outperforms Tent by 5.9%. Our sensitivity analysis reveals robust performance across various hyperparameters: prompt length L shows stability across values 1-10 (Fig. 6a), threshold ρ maintains consistent performance between 0.6-0.9 (Fig. 6b), and DPCore remains effective with as few as 50 source examples (Fig. 6c). For batch size (Fig. 6d), DPCore maintains stability above size 16 and outperforms other methods at smaller sizes, with our buffered variant DPCore-B achieving 41.2% error rate even with single-sample batches. Computationally, DPCore introduces only 0.08M parameters (0.1% of model parameters) while requiring 55.6% less computation time (Table 10). Additional results are in Appendix F.

Table 2. Effect of DPCore's three components: VPA (Visual Prompt Adaptation), PC (Prompt Coreset), and DU (Dynamic Update). Time shows relative computation time (Tent=1.0), Err Mean shows classification error rate (%).

	VPA	PC	DU	Time	Err Mean↓	Gain↑
Source	-	-	-	-	55.8	-
Tent	-	-	-	1.0	51.0	+4.8
Exp-1	✓	-	✓	1.0	50.8	+5.0
Exp-2	✓	✓	-	11.4	48.3	+7.5
Exp-3	-	✓	✓	1.6	45.1	+10.7
DPCore	✓	✓	✓	1.8	**39.9**	**+15.9**

5. Conclusion

We introduce a new CTTA setup: Continual Dynamic Change (CDC) setting that better reflects real-world scenarios where domains recur with varying frequencies and durations. Through extensive benchmarking on four datasets, we demonstrate that previous methods for CTTA struggle in CDC due to convergence issues, catastrophic forgetting, and negative transfer. To remedy this, we propose DPCore, integrating three complementary components: *Visual Prompt Adaptation* for efficient domain alignment with minimal parameters, *Prompt Coreset* for strategic knowledge preservation, and *Dynamic Update* for intelligently managing domain knowledge—updating existing prompts for similar domains while creating new ones for substantially different ones. Through our experiments, we show that DPCore is effective and achieves SOTA performance for classification and segmentation tasks for the standard CSC and the new CDC setting. Our theoretical analysis and comprehensive ablation studies further validate DPCore's effectiveness.

Impact Statements

This paper presents work whose goal is to advance the field of Machine Learning. There are many potential societal consequences of our work, none which we feel must be specifically highlighted here.

References

Ben-David, S., Blitzer, J., Crammer, K., and Pereira, F. Analysis of representations for domain adaptation. In Schölkopf, B., Platt, J., and Hoffman, T. (eds.), *Advances in Neural Information Processing Systems*, volume 19. MIT Press, 2006. URL https://proceedings.neurips.cc/paper_files/paper/2006/file/b1b0432ceafb0ce714426e9114852ac7-Paper.pdf.

Boudiaf, M., Mueller, R., Ayed, I. B., and Bertinetto, L. Parameter-free online test-time adaptation. *2022 IEEE/CVF Conference on Computer Vision and Pattern Recognition (CVPR)*, pp. 8334–8343, 2022. URL https://api.semanticscholar.org/CorpusID:246015836.

Coates, A., Ng, A., and Lee, H. An analysis of single-layer networks in unsupervised feature learning. In Gordon, G., Dunson, D., and Dudík, M. (eds.), *Proceedings of the Fourteenth International Conference on Artificial Intelligence and Statistics*, volume 15 of *Proceedings of Machine Learning Research*, pp. 215–223, Fort Lauderdale, FL, USA, 11–13 Apr 2011. PMLR. URL https://proceedings.mlr.press/v15/coates11a.html.

Dosovitskiy, A., Beyer, L., Kolesnikov, A., Weissenborn, D., Zhai, X., Unterthiner, T., Dehghani, M., Minderer, M., Heigold, G., Gelly, S., Uszkoreit, J., and Houlsby, N. An image is worth 16x16 words: Transformers for image recognition at scale. In *International Conference on Learning Representations*, 2021. URL https://openreview.net/forum?id=YicbFdNTTy.

Duda, R. O. and Hart, P. E. Pattern recognition and scene analysis, 1973.

Gan, Y., Bai, Y., Lou, Y., Ma, X., Zhang, R., Shi, N., and Luo, L. Decorate the newcomers: Visual domain prompt for continual test time adaptation. In *Proceedings of the AAAI Conference on Artificial Intelligence*, volume 37, pp. 7595–7603, 2023.

Gao, Y., Shi, X., Zhu, Y., Wang, H., Tang, Z., Zhou, X., Li, M., and Metaxas, D. N. Visual prompt tuning for test-time domain adaptation. *arXiv preprint arXiv:2210.04831*, 2022.

Gao, Y., Shi, X., Zhu, Y., Wang, H., Tang, Z., Zhou, X., Li, M., and Metaxas, D. N. Visual prompt tuning for test-time domain adaptation, 2023. URL https://openreview.net/forum?id=3HnIBTjlXTS.

Ge, C., Huang, R., Xie, M., Lai, Z., Song, S., Li, S., and Huang, G. Domain adaptation via prompt learning. *IEEE Transactions on Neural Networks and Learning Systems*, 2023.

Gong, T., Jeong, J., Kim, T., Kim, Y., Shin, J., and Lee, S.-J. NOTE: Robust continual test-time adaptation against temporal correlation. In *Advances in Neural Information Processing Systems (NeurIPS)*, 2022.

Hendrycks, D. and Dietterich, T. Benchmarking neural network robustness to common corruptions and perturbations. *arXiv preprint arXiv:1903.12261*, 2019.

Iwasawa, Y. and Matsuo, Y. Test-time classifier adjustment module for model-agnostic domain generalization. In Ranzato, M., Beygelzimer, A., Dauphin, Y., Liang, P., and Vaughan, J. W. (eds.), *Advances in Neural Information Processing Systems*, volume 34, pp. 2427–2440. Curran Associates, Inc., 2021. URL https://proceedings.neurips.cc/paper_files/paper/2021/file/1415fe9fea0fa1e45dddcff5682239a0-Paper.pdf.

Jia, M., Tang, L., Chen, B.-C., Cardie, C., Belongie, S., Hariharan, B., and Lim, S.-N. Visual prompt tuning. In *European Conference on Computer Vision*, pp. 709–727. Springer, 2022.

Kirkpatrick, J., Pascanu, R., Rabinowitz, N., Veness, J., Desjardins, G., Rusu, A. A., Milan, K., Quan, J., Ramalho, T., Grabska-Barwinska, A., et al. Overcoming catastrophic forgetting in neural networks. *Proceedings of the national academy of sciences*, 114(13):3521–3526, 2017.

Koh, P. W., Sagawa, S., Marklund, H., Xie, S. M., Zhang, M., Balsubramani, A., Hu, W., Yasunaga, M., Phillips, R. L., Gao, I., et al. Wilds: A benchmark of in-the-wild distribution shifts. In *International conference on machine learning*, pp. 5637–5664. PMLR, 2021.

Le, T., Nguyen, T., Ho, N., Bui, H., and Phung, D. Lamda: Label matching deep domain adaptation. In Meila, M. and Zhang, T. (eds.), *Proceedings of the 38th International Conference on Machine Learning*, volume 139 of *Proceedings of Machine Learning Research*, pp. 6043–6054. PMLR, 18–24 Jul 2021. URL https://proceedings.mlr.press/v139/le21a.html.

Lee, D., Yoon, J., and Hwang, S. J. Becotta: Input-dependent online blending of experts for continual test-time adaptation. In *International Conference on Machine Learning*, 2024.

Lee, D.-H. Pseudo-label : The simple and efficient semi-supervised learning method for deep neural networks. 2013.

Liang, J., Hu, D., and Feng, J. Do we really need to access the source data? source hypothesis transfer for unsupervised domain adaptation. In *International conference on machine learning*, pp. 6028–6039. PMLR, 2020.

Liang, J., He, R., and Tan, T. A comprehensive survey on test-time adaptation under distribution shifts. *arXiv preprint arXiv:2303.15361*, 2023.

Liu, C., Wang, L., Lyu, L., Sun, C., Wang, X., and Zhu, Q. Deja vu: Continual model generalization for unseen domains. *arXiv preprint arXiv:2301.10418*, 2023a.

Liu, J., Yang, S., Jia, P., Lu, M., Guo, Y., Xue, W., and Zhang, S. Vida: Homeostatic visual domain adapter for continual test time adaptation. *arXiv preprint arXiv:2306.04344*, 2023b.

Liu, J., Xu, R., Yang, S., Zhang, R., Zhang, Q., Chen, Z., Guo, Y., and Zhang, S. Continual-mae: Adaptive distribution masked autoencoders for continual test-time adaptation. pp. 28653–28663, 2024.

Liu, Z., Lin, Y., Cao, Y., Hu, H., Wei, Y., Zhang, Z., Lin, S., and Guo, B. Swin transformer: Hierarchical vision transformer using shifted windows. In *Proceedings of the IEEE/CVF international conference on computer vision*, pp. 10012–10022, 2021.

Marsden, R. A., Döbler, M., and Yang, B. Universal test-time adaptation through weight ensembling, diversity weighting, and prior correction. *2024 IEEE/CVF Winter Conference on Applications of Computer Vision (WACV)*, pp. 2543–2553, 2023. URL https://api.semanticscholar.org/CorpusID:258999734.

Mehra, A., Zhang, Y., and Hamm, J. Understanding the transferability of representations via task-relatedness. In *The Thirty-eighth Annual Conference on Neural Information Processing Systems*, 2024. URL https://openreview.net/forum?id=6cdYMkxxNt.

Mirza, M. J., Micorek, J., Possegger, H., and Bischof, H. The norm must go on: Dynamic unsupervised domain adaptation by normalization. In *Proceedings of the IEEE/CVF conference on computer vision and pattern recognition*, pp. 14765–14775, 2022.

Mirza, M. J., Soneira, P. J., Lin, W., Kozinski, M., Possegger, H., and Bischof, H. Actmad: Activation matching to align distributions for test-time-training. In *Proceedings of the IEEE/CVF Conference on Computer Vision and Pattern Recognition*, pp. 24152–24161, 2023.

Niloy, F. F., Ahmed, S. M., Raychaudhuri, D. S., Oymak, S., and Roy-Chowdhury, A. K. Effective restoration of source knowledge in continual test time adaptation. In *Proceedings of the IEEE/CVF Winter Conference on Applications of Computer Vision*, pp. 2091–2100, 2024.

Niu, S., Wu, J., Zhang, Y., Chen, Y., Zheng, S., Zhao, P., and Tan, M. Efficient test-time model adaptation without forgetting. In *International conference on machine learning*, pp. 16888–16905. PMLR, 2022.

Niu, S., Wu, J., Zhang, Y., Wen, Z., Chen, Y., Zhao, P., and Tan, M. Towards stable test-time adaptation in dynamic wild world. *arXiv preprint arXiv:2302.12400*, 2023.

Niu, S., Miao, C., Chen, G., Wu, P., and Zhao, P. Test-time model adaptation with only forward passes. In Salakhutdinov, R., Kolter, Z., Heller, K., Weller, A., Oliver, N., Scarlett, J., and Berkenkamp, F. (eds.), *Proceedings of the 41st International Conference on Machine Learning*, volume 235 of *Proceedings of Machine Learning Research*, pp. 38298–38315. PMLR, 21–27 Jul 2024. URL https://proceedings.mlr.press/v235/niu24a.html.

Recht, B., Roelofs, R., Schmidt, L., and Shankar, V. Do imagenet classifiers generalize to imagenet? In *International conference on machine learning*, pp. 5389–5400. PMLR, 2019.

Schneider, S., Rusak, E., Eck, L., Bringmann, O., Brendel, W., and Bethge, M. Improving robustness against common corruptions by covariate shift adaptation. *Advances in neural information processing systems*, 33: 11539–11551, 2020.

Shen, J., Qu, Y., Zhang, W., and Yu, Y. Wasserstein distance guided representation learning for domain adaptation. In *Proceedings of the AAAI conference on artificial intelligence*, volume 32, 2018.

Song, J., Lee, J., Kweon, I. S., and Choi, S. Ecotta: Memory-efficient continual test-time adaptation via self-distilled regularization. In *Proceedings of the IEEE/CVF Conference on Computer Vision and Pattern Recognition*, pp. 11920–11929, 2023.

Sun, J., Ibrahim, M., Hall, M., Evtimov, I., Mao, Z. M., Ferrer, C. C., and Hazirbas, C. Vpa: Fully test-time visual prompt adaptation. In *Proceedings of the 31st ACM International Conference on Multimedia*, pp. 5796–5806, 2023.

Sun, Y., Wang, X., Liu, Z., Miller, J., Efros, A., and Hardt, M. Test-time training with self-supervision for generalization under distribution shifts. In *International conference on machine learning*, pp. 9229–9248. PMLR, 2020.

Wang, D., Shelhamer, E., Liu, S., Olshausen, B., and Darrell, T. Tent: Fully test-time adaptation by entropy minimization. In *International Conference on Learning Representations*, 2021. URL https://openreview.net/forum?id=uXl3bZLkr3c.

Wang, Q., Fink, O., Van Gool, L., and Dai, D. Continual test-time domain adaptation. In *Proceedings of the IEEE/CVF Conference on Computer Vision and Pattern Recognition*, pp. 7201–7211, 2022.

Xiao, Z. and Snoek, C. G. M. Beyond model adaptation at test time: A survey, 2024. URL https://arxiv.org/abs/2411.03687.

Yang, X., Chen, X., Li, M., Wei, K., and Deng, C. A versatile framework for continual test-time domain adaptation: Balancing discriminability and generalizability. In *Proceedings of the IEEE/CVF Conference on Computer Vision and Pattern Recognition (CVPR)*, pp. 23731–23740, June 2024.

Yuan, L., Xie, B., and Li, S. Robust test-time adaptation in dynamic scenarios. In *Proceedings of the IEEE/CVF Conference on Computer Vision and Pattern Recognition*, pp. 15922–15932, 2023.

Zhang, M. M., Levine, S., and Finn, C. MEMO: Test time robustness via adaptation and augmentation. In Oh, A. H., Agarwal, A., Belgrave, D., and Cho, K. (eds.), *Advances in Neural Information Processing Systems*, 2022. URL https://openreview.net/forum?id=XrGEkCOREX2.

Zhang, Y., Mehra, A., and Hamm, J. Ot-vp: Optimal transport-guided visual prompting for test-time adaptation. *2025 IEEE/CVF Winter Conference on Applications of Computer Vision (WACV)*, 2024.

DPCore: Dynamic Prompt Coreset for Continual Test-Time Adaptation
Supplementary Materials

In the Appendix, we provide detailed supplementary materials to enhance understanding of our work:

First, we present background materials: related works on TTA and CTTA (Sec. A), comprehensive information about CTTA baselines and implementations (Sec. B), and additional details about our method and CDC setting, including hyperparameter selection and theoretical analysis (Sec. C).

The experimental aspects are covered in several sections: additional experimental results (Sec. D), discussion of our CDC setting with other CTTA settings (Sec. E), and extended ablation studies (Sec. F). Finally, we discuss limitations of our method in Sec. G.

A. Related Works

Test-Time Adaptation (TTA) (Wang et al., 2021; Iwasawa & Matsuo, 2021; Liang et al., 2020; Gao et al., 2023; Schneider et al., 2020; Mirza et al., 2022; 2023; Niu et al., 2024; Liang et al., 2023; Sun et al., 2020) enhances pre-trained model performance using unlabeled data at test time, without access to the original training phase. TTA techniques fall into two main categories based on their use of source data. The first adjusts models through self-supervised losses like entropy minimization (Wang et al., 2021; Niu et al., 2023) and consistency maximization (Wang et al., 2022; Liu et al., 2023b; 2024). The second involves preliminary steps using source data: either by extracting source characteristics such as statistics or features (Mirza et al., 2023; Niu et al., 2024; Zhang et al., 2024)) or by warming up injected parameters on source data before adaptation (Lee et al., 2024; Song et al., 2023; Gan et al., 2023; Liu et al., 2023b; Gao et al., 2023).

Crucially, both approaches are source-free adaptation since they operate without source data during adaptation. While our method falls into the second category, it significantly reduces source dependency compared to existing methods: DPCore requires only 300 unlabeled source examples to compute statistics, in contrast to DePT (Gao et al., 2023), ViDA (Liu et al., 2023b), VDP (Gan et al., 2023) and BeCoTTA (Lee et al., 2024) which need the entire source dataset for warm-up. Moreover, as demonstrated in Fig. 6c, our approach maintains effectiveness even when source data is completely unavailable.

Continual Test-Time Adaptation (CTTA) (Wang et al., 2022; Lee et al., 2024; Niu et al., 2022; Niloy et al., 2024; Liu et al., 2023a; Boudiaf et al., 2022; Gong et al., 2022; Yuan et al., 2023) tackles the challenge of non-stationary target domains. This paradigm was first introduced in (Wang et al., 2022), referred to as CSC in this work and shown in the top of Fig. 1, where domains change in a structured manner with clear boundaries and uniform lengths. While several works (Niu et al., 2023; Boudiaf et al., 2022; Gong et al., 2022) explore TTA challenges such as mixed domains and label imbalance, they primarily focus on the static domain. (Yuan et al., 2023) extends this exploration to the CSC setting, investigating label imbalance within batches from changing domains. More recently, (Lee et al., 2024) introduced scenarios with continual gradual shifts, where domain boundaries become blurred and transitional batches may contain mixed-domain data, though the overall domain progression still follows the CSC pattern.

Existing methods often overlook frequent domain changes and irregular durations, which are critical in real-world applications. To address this gap, we propose the Continual Dynamic Change (CDC) setting, where domains change in a more realistic, dynamic manner. Traditional CTTA methods struggle in this setting, as demonstrated in Fig. 4b. Our DPCore is specifically designed to mitigate the effect of diverse domain change patterns and frequencies.

B. Baselines

In this section, we provide the details of the CTTA baselines we use in our paper.

Tent[1] **(Wang et al., 2021)** updates the Norm Layer parameters through prediction entropy minimization. We follow the same hyperparameters that are set in Tent.

CoTTA[2] **(Wang et al., 2022)** is the first to perform TTA on continually changing domains and propose a teacher-student learning scheme with augmentation-based consistency maximization. We follow the same hyperparameters that are set in CoTTA. The trainable parameters are all the parameters in ViT-Base.

DePT (Gao et al., 2023) integrates visual prompts with Vision Transformers to adapt to target domains through memory bank-based pseudo-labeling. This method utilizes

[1] https://github.com/DequanWang/tent
[2] https://github.com/qinenergy/cotta

a significant number of prompts, which are initialized by warming up on source data.

SAR[3] **(Niu et al., 2023)** introduces a sharpness-aware and reliable entropy minimization method. This approach selectively filters noisy samples and optimizes model weights towards stable regions in the parameter space.

VDP (Gan et al., 2023) employs visual domain prompts in pixel space to adapt to continually changing domains. It dynamically updates lightweight prompts to facilitate domain adaptation, modifying input images instead of model parameters. The pixel prompts are initialized on source data.

EcoTTA[4] **(Song et al., 2023)** utilizes lightweight meta networks and self-distilled regularization to maintain memory efficiency and ensure long-term adaptation stability. This method emphasizes consistency between the outputs of meta networks and the original frozen network, with meta-networks warmed up on source data for several epochs.

ViDA[5] **(Liu et al., 2023b)** uses high-rank and low-rank domain adapters to manage domain-specific and shared knowledge. Designed to address continual test-time adaptation, it dynamically responds to changing domain conditions. The adapters are warmed up on source data.

BDG (Yang et al., 2024) is a framework designed to balance discriminability and generalization in CTTA by generating high-quality supervisory signals. This framework uses adaptive thresholds for pseudo-label reliability, leverages knowledge from a pre-trained source model to adjust unreliable signals, and calculates a diversity score to ensure future domain generalization.

C-MAE[6] **(Liu et al., 2024)** introduces Adaptive Distribution Masked Autoencoders for CTTA, which employ a Distribution-aware Masking mechanism to adaptively sample masked positions in images.

We utilize official implementations of the method where available; otherwise, we implement it ourselves using the hyperparameters reported in the original paper. To ensure fair comparison, we maintain consistent hyperparameters across both CSC and CDC settings.

C. Additional Details of DPCore

C.1. Visual Prompt Adaptation in TTA

In the context of TTA where labels are unavailable, prompts can be optimized through consistency maximization, entropy minimization, or unsupervised distribution alignment (Niu et al., 2024; Sun et al., 2023; Gao et al., 2023; Zhang et al., 2024). We employ distribution alignment due to its proven effectiveness and computational simplicity (Ben-David et al., 2006; Mehra et al., 2024).

For the current batch B_t^T at time step t from unknown target domain T, a prompt is optimized by minimizing the distribution alignment between source and target features:

$$\boldsymbol{p}^* = \arg\min_{\boldsymbol{p}} \ d(\mathcal{Z}^S, \mathcal{Z}_t^T(\boldsymbol{p})) \tag{7}$$

where d represents a distribution distance and $\mathcal{Z}_t^T(\boldsymbol{p}) = \phi(B_t^T; \theta_\phi, \boldsymbol{p})$ denotes the extracted features of the current batch with prompt $\boldsymbol{p}$, as shown on the right of Fig. 2. We employ marginal distribution alignment (Ben-David et al., 2006; Le et al., 2021; Shen et al., 2018) to avoid potential error accumulation from pseudo labels in continual learning scenarios, though other sophisticated distance metrics are also applicable.

Unlike previous prompt-based TTA methods such as DePT (Gao et al., 2023) or VDP (Gan et al., 2023) that require prompt warm-up on source data for optimal initialization, we initialize prompt tokens from a Gaussian distribution without any warm-up, following Visual Prompt Tuning in supervised settings (Jia et al., 2022). This approach makes our method more practical and efficient.

C.2. Algorithm of DPCore

To illustrate how DPCore operates as shown in Fig. 2, we present its complete algorithm in Alg. 1.

C.3. Implementation Details

Here we detail the hyperparameters used in our main experiments. We randomly sample 300 source examples to compute the statistics and set the number of prompt tokens to 8 with a test batch size of 64. The updating weight is set as $\alpha = 0.999$. We learn the prompt from scratch for 50 steps and refine the existing prompt for only 1 step. The model is optimized using AdamW with a learning rate of 0.01, and the threshold ρ is set to 0.8. These hyperparameters were determined using four disjoint validation corruptions from ImageNet-C and CIFAR10-C (Hendrycks & Dietterich, 2019): [Speckle Noise, Gaussian Blur, Spatter, Saturate], following (Zhang et al., 2022).

For datasets without validation sets (e.g., CIFAR100-to-CIFAR100C and Cityscapes-to-ACDC), we apply these same hyperparameters without additional tuning to align with practical testing conditions, where hyperparameters must be selected prior to accessing target data. Moreover, we employ identical hyperparameters across both CSC and CDC settings.

[3]https://github.com/mr-eggplant/SAR
[4]https://github.com/Lily-Le/EcoTTA
[5]https://github.com/Yangsenqiao/vida
[6]https://github.com/RanXu2000/continual-mae

Algorithm 1 The proposed algorithm DPCore

Input: A source pre-trained model $f(x)$, source statistics Γ^S, test batches $\{B_t\}_{t=1}^T$
Initialization: An empty coreset, a pre-defined ratio threshold ρ, and random prompt tokens.

```
1:  for the first batch $B_1$ do
2:      Compute the statistics of batch $B_1$ without prompt.
3:      Learn prompt from scratch (Eq. 7).
4:      Add the batch statistics and prompt to the empty coreset.
5:  end for
6:  for $t = 2, ..., T$ do
7:      Compute the statistics of batch $B_t$ without prompt.
8:      Compute the weights and weighted prompts (Eq. 5).
9:      Compute batch statistics with the weighted prompt.
10:     Compute ratio of distances with/w.o. weighted prompt.
11:     if ratio $\leq \rho$ then
12:         Update weighted prompt on $B_t$ by 1 step.
13:         Update all coreset elements (Eq. 6).
14:     else
15:         Learn prompt from scratch for $B_t$ (Eq. 7).
16:         Add the batch statistics and learned prompt to the coreset
            as a new element.
17:     end if
18: end for
```

Output: Prediction for all batches; The learned coreset.

C.4. Comprehensive Analysis of DPCore

We elaborate on the theoretical analysis introduced in Sec. 3. For simplicity, we consider a version of Alg. 1 where we use one-hot weights instead of general weights—only the closest core element to a given test batch is considered, and only the mean is stored in the coreset. The simplified algorithm is presented in Alg. 2, denoted as $\mathcal{A}$

Consider batches $B_1, ..., B_t$ naturally clustered into M mutually exclusive clusters $\{G^i\}_{i=1}^M$ based on their distances. Let $\text{Conv}(G^i)$ be the convex hull of batches in G^i, $\text{diam}(S) = \sup_{x,x' \in S} d(x, x')$ be the diameter of set S, and $d(S, S') = \inf_{x \in S, x' \in S'} d(x, x')$ be the set distance. We denote by $\Pi^{(t-1)}$ the set of permutations on $(1, ..., t-1)$, by G_t^i the set of batches in cluster i at time t, and by $\{\boldsymbol{p}_t^i, \boldsymbol{\mu}_t^i\}$ the i-th core element at time t. Each core element consists of a core prompt $\boldsymbol{p}_t^i$ and a core mean $\boldsymbol{\mu}_t^i$. Abstractly, the algorithm $\mathcal{A}$ generates the current prompt $\boldsymbol{p}_t = \mathcal{A}(\{B_{t-1}, ..., B_1\})$ using the batch history $\{B_1, ..., B_{t-1}\}$ as input.

Assumption (Well-separated clusters): There exists $\theta > 0$ such that:

$$\text{diam}(\text{Conv}(G^i)) < \theta < d(\text{Conv}(G^i), \text{Conv}(G^j)), \ \forall i \neq j$$

This implies batches within the same cluster are closer to each other than to batches from different clusters.

Proposition C.1. *For any $t \geq 1$, Alg. 2 assigns all batches $B_1, ..., B_t$ to correct clusters.*

Proof. We prove by induction. At $t = 1$, since no clusters exist, B_1 creates the first cluster with $\boldsymbol{\mu}^1 = \boldsymbol{\mu}(B_1)$. Suppose cluster assignments are correct for batches $B_1, ..., B_{t-1}$. Since each core mean $\boldsymbol{\mu}^i$ is updated through interpolation $(1-\alpha)\boldsymbol{\mu}^i + \alpha\boldsymbol{\mu}(B_t)$, it remains within the convex hull of its cluster: $\boldsymbol{\mu}_t^i \in \text{Conv}(G_t^i)$.

When a new batch B_t belonging to cluster j arrives, we consider four cases based on whether cluster j or other clusters contain batches: 1) If no clusters exist ($|G_{t-1}^j| = |G_{t-1}^k| = 0, \ \forall k \neq j$), B_t creates a new cluster. 2) If only other clusters exist ($|G_{t-1}^j| = 0, \text{ and } \exists k \neq j : |G_{t-1}^k| > 0$), well-separatedness ensures $d(\boldsymbol{\mu}(B_t), \boldsymbol{\mu}^k) > \theta$, so B_t creates a new cluster. 3) If only cluster j exists ($|G_{t-1}^j| > 0, \text{ and } |G_{t-1}^k| = 0, \ \forall k \neq j$), well-separatedness ensures $d(\boldsymbol{\mu}(B_t), \boldsymbol{\mu}^j) < \theta$, so B_t joins cluster j. 4) If multiple clusters exist ($|G_{t-1}^j| > 0, \text{ and } \exists k \neq j : |G_{t-1}^k| > 0$), well-separatedness ensures $d(\boldsymbol{\mu}(B_t), \boldsymbol{\mu}^j) < \theta < d(\boldsymbol{\mu}(B_t), \boldsymbol{\mu}^k)$, so B_t correctly joins cluster j. □

Proposition C.2. *For any $t > 1$, Alg. 2 assigns B_t to the correct cluster independent of batch order $B_{\pi(1)}, ..., B_{\pi(t-1)}, \forall \pi \in \Pi^{(t-1)}$. Furthermore, if $\alpha = \frac{1}{|G^j|}$, then the core mean is the cluster mean: $\boldsymbol{\mu}_t^i = \frac{1}{|G_t^i|} \sum_{B \in G_t^i} \boldsymbol{\mu}(B)$, also independent of batch order.*

Proof. From Proposition C.1, correct assignment at time t depends only on well-separatedness and correct assignments at $t-1$, not on batch order. For the second claim, consider batches $B^{(1)}, B^{(2)}, ...$ are the batches assigned to cluster j in the order they are processed. With $\alpha = \frac{1}{|G^j|}$, updates yield: $\boldsymbol{\mu}^j = \boldsymbol{\mu}(B^{(1)})$, $\boldsymbol{\mu}^j = \frac{1}{2}(\boldsymbol{\mu}(B^{(1)}) + \boldsymbol{\mu}(B^{(2)}))$, $\boldsymbol{\mu}^j = \frac{1}{3}(\boldsymbol{\mu}(B^{(1)}) + \boldsymbol{\mu}(B^{(2)}) + \boldsymbol{\mu}(B^{(3)}))$, and so on. This running average is independent of batch order. □

Proposition C.3. *For any $t > 1$, Alg. 2 learns prompt $\boldsymbol{p}_t$ for batch B_t independent of batch order $B_{\pi(1)}, ..., B_{\pi(t-1)}, \forall \pi \in \Pi^{(t-1)}$.*

Proof. From Proposition C.2, cluster assignment is independent of batch order. For batch B_t, two cases arise: 1) If B_t belongs to an existing cluster i, $\boldsymbol{p}_t$ is learned starting from existing core prompt $\boldsymbol{p}^i$. Since $\boldsymbol{p}^i$ is order-independent, $\boldsymbol{p}_t$ is also order-independent. 2) If B_t creates a new cluster, $\boldsymbol{p}_t$ is learned from scratch, making it inherently order-independent. □

Our analysis demonstrates three key properties of DPCore under the well-separatedness assumption: 1) Correct Clustering: DPCore correctly assigns all batches to their respective clusters regardless of sequence length. 2) Order Independence: Cluster assignments remain correct regardless of the order in which batches arrive. 3) Prompt Stability: The learned prompts are independent of batch order.

These properties together show that DPCore can effectively manage domain knowledge even when domains appear in arbitrary orders—a crucial advantage in dynamic environments. While this analysis uses simplified assumptions, it provides valuable insight into DPCore's robustness to random domain changes. The full analysis under general conditions remains an interesting direction for future work.

Algorithm 2 A simplified version of the proposed algorithm

```
1: for $t = 1, 2, ..., T$ do
2:     Compute the batch mean $\boldsymbol{\mu}(B_t)$ and distances $d^j = d(\boldsymbol{\mu}(B_t), \boldsymbol{\mu}^j),\ i = 1, ..., K$ against all existing core elements.
3:     if coreset is empty or $\min_j d^j > \theta$ then
4:         Learn prompt from scratch for $B_t$ (Eq. 7).
5:         Add the batch mean and learned prompt to the coreset as a new element.
6:     else
7:         Assign $B_t$ to the closest core element $j^* = \arg\min_j d^j$.
8:         Update the prompt in $j^*$-th core element by 1 step.
9:         Update $j^*$-th core element (Eq. 6).
10:    end if
11: end for
Output: Prediction for all batches; The learned coreset.
```

D. Additional Results

D.1. Performance of Single Domain-learned Prompt

To validate the core intuition behind DPCore, we conduct a preliminary experiment examining how a prompt learned from one domain transfers to others. Specifically, we learn a prompt from scratch on the Gaussian Noise domain and evaluate its effectiveness across the remaining 14 domains. For comparison, we also learn domain-specific prompts independently with known domain boundaries, where the model resets each time it encounters a new domain. As shown in Table 3, the Gaussian Noise-learned prompt yields interesting transfer patterns: it significantly improves performance on similar domains (Shot Noise and Impulse Noise), shows limited effectiveness on others (Defocus Blur and Elastic), and even degrades performance on substantially different domains (Motion and Contrast). These performance variations strongly align with the domain distance measurements illustrated in Fig. 3a, suggesting that the effectiveness of prompt transfer is directly related to the similarity of domains in feature space.

Notably, DPCore surprisingly outperforms the domain-specific prompts despite requiring no domain boundary information. This superior performance stems from DPCore's ability to learn a unified prompt for similar domains (e.g., the entire Noise group including Gaussian, Shot, and Impulse), achieving better adaptation than learning from individual domains in isolation.

These empirical findings reveal two crucial insights that motivate DPCore's design: (1) prompts can transfer effectively between similar domains, potentially enabling more efficient adaptation, and (2) for fundamentally different domains, learning new domain-specific prompts is essential to prevent negative transfer.

D.2. Results for 10 Random Orders in CSC

This section provides details for the results presented in Fig. 3c. We strictly follow the ten random orders used in CoTTA (Wang et al., 2022) and evaluate DPCore on ImageNet-to-ImageNet-C across all ten domain orders. It is important to note that even though the domain order is changed, the domain change frequency and domain length remain fixed, resulting in the same domain change pattern in CSC setting. DPCore demonstrates robust performance in this setting, achieving an average error rate of 40.2% with an average coreset size of 13.9 elements. These results highlight the consistency and effectiveness of DPCore across various domain orders, further validating its applicability in real-world scenarios where the order of encountered domains may vary.

D.3. Results for CIFAR10/100-to-CIFAR10/100C

In this section, we present the results on CIFAR10/100-to-CIFAR10/100C across both CSC and CDC settings. The results for CIFAR10-to-CIFAR10C are in Table 4 and Table 5 for CSC and CDC settings respectively. In the CSC setting, DPCore significantly outperforms all existing methods, achieving a +12.8% improvement over the source pre-trained model and surpassing the previous SOTA (ViDA) by 5.3%. This improvement is consistent across all corruption types, with particularly strong performance on noise corruptions (reducing error rates from 60.1% to 22.0% on Gaussian Noise). In the more challenging CDC setting, while previous methods show substantial degradation (ViDA's improvement drops from +7.5% to +4.6%), DPCore maintains robust performance with an 11.1% improvement over the source model.

Similarly, for CIFAR100-to-CIFAR100C task (results in Tables 11 and 12), DPCore demonstrates strong performance across both settings. In CSC, DPCore achieves a 10.3% improvement over the source model and outperforms ViDA by 2.2%, with notable improvements across all corruption types, particularly on Glass (44.1% vs 60.5% source error rate) and Contrast corruptions (13.2% vs 34.8% source error rate). The CDC setting presents a greater challenge, where several methods (CoTTA, VDP) perform worse than the source model, and ViDA's improvement drops from +8.1% to +5.6%. In contrast, DPCore maintains robust perfor-

Table 3. **Classification error rate (%) for ImageNet-to-ImageNet-C in the CSC setting.** Gaussian Noise-learned Prompt denotes the prompt learned solely on Gaussian Noise and evaluated across other domains. Domain-specific prompt denote the prompt learned on each domain separately with known domain boundary.

Algorithm	Gauss.	Shot	Impulse	Defocus	Glass	Motion	Zoom	Snow	Frost	Fog	Bright	Contrast	Elastic	Pixel	JPEG	Mean↓	Gain↑
Source	53.0	51.8	52.1	68.5	78.8	58.5	63.3	49.9	54.2	57.7	26.4	91.4	57.5	38.0	36.2	55.8	0.0
Tent	52.2	48.9	49.2	65.8	73.0	54.5	58.4	44.0	47.7	50.3	23.9	72.8	55.7	34.4	33.9	51.0	+4.8
Gaussian Noise-learned Prompt	42.2	40.4	42.1	67.5	65.3	60.4	66.8	50.0	41.2	56.8	27.6	95.7	56.3	37.7	32.6	52.2	+3.6
Domain-specific Prompt	42.2	39.9	41.6	58.8	58.1	48.6	44.0	35.0	40.6	41.5	21.1	42.9	45.6	29.6	28.0	41.2	+14.6
DPCore (Proposed)	**42.2**	**38.7**	**39.3**	**47.2**	**51.4**	**47.7**	**46.9**	**39.3**	**36.9**	**37.4**	**22.0**	**44.4**	**45.1**	**30.9**	**29.6**	**39.9**	**+15.9**

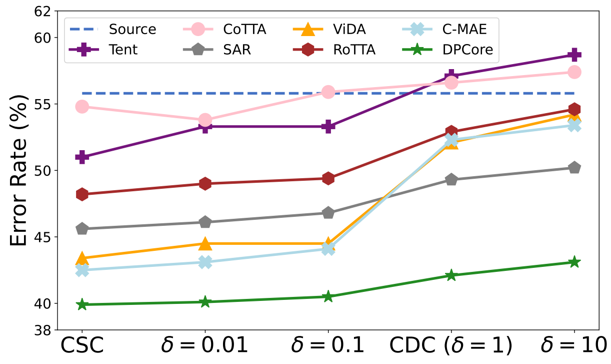

Figure 5. Performance comparison across different domain change patterns on ImageNet-to-ImageNet-C. The x-axis shows settings from CSC to CDC with increasing Dirichlet parameter δ, where larger δ indicates more frequent domain changes. DPCore maintains stable performance even with rapid domain transitions, while other methods degrade significantly.

mance with an 8.0% improvement over the source model, demonstrating its effectiveness.

D.4. Comprehensive Results for Cityscapes-to-ACDC

Beyond classification, we evaluate DPCore on real-world semantic segmentation using the Cityscapes-to-ACDC dataset, where performance is measured by mean Intersection over Union (mIoU, %). In this section, we provide fine-grained results on Cityscapes-to-ACDC, presented in Table 13 and Table 14 for CSC and CDC settings respectively. In the CSC setting following (Liu et al., 2023b; 2024) where domain sequences repeat three times, DPCore shows consistent improvement in mIoU across cycles (62.1 $\rightarrow$ 62.6 $\rightarrow$ 62.8), outperforming previous SOTA ViDA by 0.6%. In the more challenging CDC setting, while Tent and EcoTTA perform worse than the source model and ViDA's improvement drops from +5.2% to +2.5%, DPCore maintains robust performance (from +5.8% to +4.3%) while adapting its coreset size from 5 elements in CSC to 7 in CDC to handle increased domain complexity. Fine-grained results are available in Appendix D.4.

E. Discussion on CTTA Setting.

E.1. CDC with Different Dirichlet Distributions

We analyze how different domain change patterns affect CTTA methods by varying the Dirichlet distribution parameter δ that controls our CDC simulation. As shown in Fig. 5, smaller δ values (0.01, 0.1) produce domain changes more similar to CSC, while larger values (1, 10) lead to increasingly frequent transitions. DPCore demonstrates remarkable stability across all settings, with error rates increasing only modestly from 39.9% (CSC) to 43.1% ($\delta = 10$), consistently outperforming previous SOTA methods. The stability of other methods, however, deteriorates significantly as δ increases. In the most challenging scenario ($\delta = 10$) where domains change most rapidly, most previous methods perform similarly to or worse than the source model (55.8%). While SAR maintains some improvement with 50.2% error rate, DPCore significantly outperforms all methods with 43.1%, demonstrating its robust adaptation capability even under extreme domain variation.

E.2. CDC with Other Distributions

To provide a comprehensive understanding of our CDC setting beyond the Dirichlet distribution, we present a sequence generation method based on two independent distributions: one for domain selection and another for domain duration (number of batches), termed as **CDC-2D**. This two-distribution approach allows us to flexibly control both which domains appear and how long they persist, creating realistic scenarios of domain changes.

Taking uniform distributions as a simple case, we iteratively construct the domain sequence through the following process: at each step, we randomly select a domain from the domain pool using uniform probability, then randomly determine the number of consecutive batches to assign to this domain, also using uniform distribution. If a selected domain has no remaining batches, we perform reselection until finding an available domain. This process continues until all batches across all domains have been assigned, naturally ensuring unpredictable domain changes with varying durations while maintaining complete coverage of all domains.

This uniform distribution-based generation, which we term

Table 4. **Classification error rate (%) for CIFAR10-to-CIFAR10C in the CSC setting.**

Algorithm	Gauss.	Shot	Impulse	Defocus	Glass	Motion	Zoom	Snow	Frost	Fog	Bright	Contrast	Elastic	Pixel	JPEG	Mean↓	Gain↑
Source	60.1	53.2	38.3	19.9	35.5	22.6	18.6	12.1	12.7	22.8	5.3	49.7	23.6	24.7	23.1	28.2	0.0
Tent (Wang et al., 2021)	57.7	56.3	29.4	16.2	35.3	16.2	12.4	11.0	11.6	14.9	4.7	22.5	15.9	29.1	19.5	23.5	+4.7
CoTTA (Wang et al., 2022)	58.7	51.3	33.0	20.1	34.8	20	15.2	11.1	11.3	18.5	4.0	34.7	18.8	19.0	17.9	24.6	+3.6
VDP(Gan et al., 2023)	57.5	49.5	31.7	21.3	35.1	19.6	15.1	10.8	10.3	18.1	4	27.5	18.4	22.5	19.9	24.1	+4.1
ViDA (Liu et al., 2023b)	52.9	47.9	19.4	11.4	31.3	13.3	7.6	7.6	9.9	12.5	3.8	26.3	14.4	33.9	18.2	20.7	+7.5
DPCore(Proposed)	**22.0**	**18.2**	**14.9**	**14.3**	**24.4**	**13.9**	**12.0**	**11.6**	**10.7**	**15.0**	**5.7**	**21.8**	**15.6**	**12.7**	**18.0**	**15.4**	**+12.8**

Table 5. **Classification error rate (%) for CIFAR10-to-CIFAR10C in the CDC setting.**

Algorithm	Gauss.	Shot	Impulse	Defocus	Glass	Motion	Zoom	Snow	Frost	Fog	Bright	Contrast	Elastic	Pixel	JPEG	Mean↓	Gain↑
Source	60.1	53.2	38.3	19.9	35.5	22.6	18.6	12.1	12.7	22.8	5.3	49.7	23.6	24.7	23.1	28.2	0.0
Tent (Wang et al., 2021)	57.4	51.7	34.2	18.2	35.1	22.4	16.9	11.8	12.6	21.6	5.1	36.7	22.1	24.3	23.2	26.2	+2.0
CoTTA (Wang et al., 2022)	59.2	54.8	45.1	20.5	36.1	21.9	19.1	11.6	12.1	21.2	6.1	35.1	22.5	21.7	19.7	27.1	+1.1
VDP(Gan et al., 2023)	58.1	51.2	32.2	22.4	34.8	20.4	15.6	11.2	11.4	20.1	4.9	30.4	20.4	22.7	19.9	25.0	+3.2
ViDA (Liu et al., 2023b)	56.4	50.8	28.4	16.7	32.5	15.2	13.7	10.1	10.4	13.5	4.2	26.5	19.4	35.1	21.2	23.6	+4.6
DPCore(Proposed)	**24.1**	**20.6**	**24.5**	**13.9**	**26.5**	**14.2**	**13.2**	**13.4**	**10.2**	**12.8**	**5.0**	**22.5**	**16.8**	**20.1**	**18.5**	**17.1**	**+11.1**

CDC-2D, offers an alternative perspective on dynamic domain changes compared to the Dirichlet approach in the main paper. As shown in Table 7, we observe two significant trends similar to our main results: First, previous SOTA methods suffer substantial performance degradation when moving from CSC to this CDC-2D setting, with several methods showing minimal improvement over the source model's 55.8% error rate and even the best baseline achieving only moderate gains. This degradation is particularly evident in challenging corruption types where most methods struggle to significantly improve upon the source model. Second, DPCore maintains robust performance with a 43.2% error rate (comparable to 42.1% achieved with Dirichlet distribution) and consistently outperforms other methods, achieving a significant improvement of +12.6% over the source model while the second-best method only achieves +8.1

To further validate DPCore's effectiveness across diverse domain change patterns, we explore CDC settings with different probability distributions. Taking ImageNet-to-ImageNet-C as an example with its 15 corruption domains, we consider probability vectors $[P_1, P_2, ..., P_{15}]$ where each P_i represents the probability of selecting the i-th domain. These vectors must satisfy $P_i > 0$ for all i (ensuring every domain has some probability of being selected) and $\sum_{i=1}^{15} P_i = 1$ (making it a valid probability distribution). The uniform distribution represents a special case where $P_i = \frac{1}{15}$ for all i. We randomly generate ten different such probability vectors, each defining a unique pattern of domain changes. The results in Table 7 demonstrate DPCore's remarkable consistency across these varied settings, achieving a mean error rate of 43.5% with standard deviation of 0.7. This stability across different domain change patterns further validates DPCore's robustness and its ability to handle diverse scenarios of distribution shift.

E.3. Comparison with Other CTTA Settings

In this section, we discuss how our proposed CDC setting differs from other CTTA variants. First, we consider the repeating setting introduced in (Wang et al., 2022), where 15 corruption domains are repeated for 10 rounds. While this setting eventually accumulates numerous domain changes, it differs fundamentally from CDC: each domain maintains uniform duration (782 batches), and changes occur gradually. This structured nature makes it more similar to CSC than our CDC setting, where domain durations vary significantly and changes occur more frequently.

Second, the gradual domain change setting proposed in (Lee et al., 2024) assumes blurred domain boundaries, where batches near transitions contain mixed-domain data. While this realistic assumption differs from traditional CTTA methods, it still follows the CSC pattern where mixed batches constitute only a small portion of all data due to long domain durations. Although we haven't directly evaluated DPCore in this setting, our proposed variant DPCore-B (detailed in Section F.2) demonstrates effective handling of mixed-domain batches, suggesting potential applicability to gradual domain changes.

Third, the Practical Test-Time Adaptation (PTTA) setting (Yuan et al., 2023) assumes label-balanced batches with local class correlation (e.g., single-class batches) in CSC. This contrasts with our setting, which follows the common CTTA assumption (Wang et al., 2022; Niu et al., 2022; Liu et al., 2023b; 2024) of uniform sampling and label balance. Interestingly, despite not being designed for PTTA, DPCore shows substantial improvement in this setting (results in Table 8). Meanwhile, RoTTA (Yuan et al., 2023), though specifically designed for PTTA, demonstrates limited effectiveness on ImageNet-C with ViTs compared to its stronger performance on smaller datasets like CIFAR10, consistent with findings in (Marsden et al., 2023). Further-

Table 6. **Classification error rate (%) for ImageNet-to-ImageNet-C in the CDC-2D setting.**

Algorithm	Gauss.	Shot	Impulse	Defocus	Glass	Motion	Zoom	Snow	Frost	Fog	Bright	Contrast	Elastic	Pixel	JPEG	Mean↓	Gain↑
Source	53.0	51.8	52.1	68.5	78.8	58.5	63.3	49.9	54.2	57.7	26.4	91.4	57.5	38.0	36.2	55.8	0.0
Tent (Wang et al., 2022)	54.1	53.2	52.9	66.7	74.6	56.6	61.2	49.2	52.3	57.5	32.1	90.4	56.1	37.7	37.1	55.4	+0.4
CoTTA (Wang et al., 2022)	52.4	52.2	51.1	68.4	76.3	57.9	62.1	48.7	53.1	55.1	26.1	88.9	57.1	37.6	38.2	55.0	+0.8
VDP (Gan et al., 2023)	53.1	53.3	51.5	62.4	73.1	53.4	60.1	43.5	54.3	58.2	25.1	82.2	56.6	35.7	36.3	53.3	2.5
SAR (Niu et al., 2023)	47.0	46.1	46.1	56.1	66.4	49.9	55.1	41.1	44.8	50.9	23.6	65.3	54.2	32.9	31.4	47.4	+8.1
EcoTTA (Song et al., 2023)	48.9	47.4	49.3	59.2	71.2	54.1	59.8	46.2	44.3	57.2	24.0	84.1	55.2	37.2	35.3	51.6	+4.2
ViDA (Liu et al., 2023b)	48.8	49.2	47.3	56.6	71.6	55.3	59.6	41.2	49.4	60.5	27.1	83.9	57.9	34.6	34.4	51.8	+4.0
DPCore (Proposed)	**42.7**	**40.4**	**42.2**	**57.4**	**61.0**	**51.1**	**52.4**	**35.8**	**41.0**	**38.8**	**22.1**	**55.4**	**48.3**	**31.1**	**28.1**	**43.2**	**+12.6**

Table 7. **Average error rate (%) of DPCore across 10 different CDC-2D settings (R1-10) on ImageNet-to-ImageNet-C.**

	Source	Uniform	R1	R2	R3	R4	R5	R6	R7	R8	R9	R10	**Average**	**Std**
Err Mean↓	55.8	43.2	42.1	42.8	44.2	43.5	43.5	42.7	43.9	44.4	44.7	43.0	43.5	0.7

Table 8. Average error rate (%) of DPCore and RoTTA across various CTTA settings on ImageNet-to-ImageNet-C. The improvement over the source model is shown in parentheses.

Algorithm	CSC	PTTA	CDC	Average
Source	55.8	55.8	55.8	0
RoTTA	48.2 (+7.6)	49.5 (+6.35)	53.1 (+2.7)	50.3 (+5.6)
DPCore	**39.9 (+15.9)**	**43.9 (+12.0)**	**42.1 (13.7)**	**42.0 (+13.9)**

Table 9. Average error rate (%) of DPCore-B across various buffer zone size D on ImageNet-to-ImageNet-C in CSC setting when batch size is one.

	Source	D= 8	D= 16	D= 32	D= 64
Err Mean↓	55.8	43.0	42.1	41.6	41.2

more, RoTTA's performance degrades significantly in our CDC setting. In contrast, DPCore maintains robust performance across CSC, CDC, and PTTA settings, demonstrating its versatility across different test-time scenarios.

Our CDC setting introduces unique challenges through its combination of frequent domain changes and varying domain durations, distinguishing it from previous CTTA variants. This more dynamic and unpredictable environment better reflects real-world scenarios while posing significant challenges for existing CTTA methods.

F. Additional Ablation Studies

F.1. Ablation Studies

We provide comprehensive analyses and ablation studies for DPCore on ImageNet-to-ImageNet-C in the CSC setting. Additional results are available in Appendix F.

Effect of Each Component. Table 2 evaluates the contributions of DPCore's key components: Visual Prompt Adaptation (VPA), Prompt Coreset (PC), and Dynamic Update (DU). In the first experiment (Exp-1), employing only VPA and DU without PC, we see a 4.8% reduction in error rate compared to the source pre-trained model, with computation time similar to Tent as it involves learning a single prompt from scratch for all domains. Exp-2 introduces PC but omits DU, requiring new prompts for each batch, enhancing performance to +7.5% but increasing computation time tenfold compared to Tent. In Exp-3, we replace VPA with NormLayer parameters while retaining PC and DU, outperforming Tent by +5.9%, illustrating the method's adaptability beyond ViT architectures to CNNs by adapting NormLayer parameters. The full DPCore setup, integrating VPA, PC, and DU, achieves a SOTA improvement of +15.9% while maintaining computational efficiency.

Effect of prompt length L. We assess the impact of prompt size by varying the number of prompt tokens L within the range of $\{1, 2, ..., 10\}$. As depicted in Fig. 6a, DPCore's performance exhibits strong stability across different values of L, demonstrating low sensitivity to this parameter. We fix $L = 8$ for all main experiments.

DPCore's sensitivity to threshold ρ. The threshold ρ in Alg. 1 controls DPCore's sensitivity to domain changes. Lower ρ values result in more batches being classified as samples from unseen domains. For example, setting ρ near zero causes each batch to learn its own prompt. In contrast, high ρ values lead to all batches after the first one being considered as from visited domains, potentially reducing the coreset to a single element. However, even a high ratio ρ such as 1 is likely to learn a new core element if the weighted prompt $\boldsymbol{p}_w$ increases the domain gap significantly for different unseen domains, i.e., $d(\Gamma^S, \Gamma_t(\boldsymbol{p}_w)) > d(\Gamma^S, \Gamma_t)$. We examine ρ within a range of 0.1 to 1.0. Experimental results, as shown in Fig. 6b, demonstrate stable performance for ρ values from 0.6 to 0.9. To ensure consistency and avoid dataset-specific tuning, we fix $\rho = 0.8$ across all our main experiments before any exposure to target data.

Effect of test batch size. To comprehensively assess the impact of test batch size, we evaluate various CTTA meth-

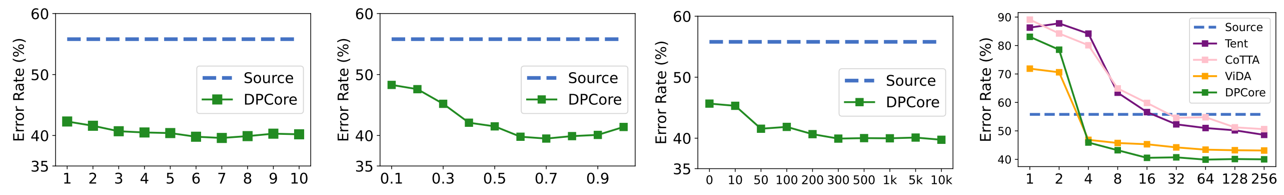

(a) Prompt Length L (b) Threshold Ratio ρ (c) Number of Source Examples (d) Batch Size

Figure 6. Ablation studies on ImageNet-to-ImageNet-C: impact of (a) prompt token length, (b) threshold ratio for core element evaluation, (c) number of source examples used for statistics computation, and (d) batch size on classification error rate.

ods across batch sizes ranging from 1 to 256. The results illustrated in Fig. 6d reveal a consistent pattern across methods: regardless of their objective functions (entropy, consistency, or distribution alignment), they maintain stable performance with sufficiently large batch sizes but exhibit increased error rates as batch sizes decrease. In the extreme case of single-sample adaptation (batch size one), all methods demonstrate significantly degraded performance, falling below the source model's baseline. This observation aligns with findings reported in recent literature (Yuan et al., 2023; Song et al., 2023). Based on these empirical findings and consistent with prior work, we standardize the batch size to 64 for fair comparison across methods. Moreover, DPCore maintains exceptional stability for batch sizes above 16 and shows minimal degradation for smaller sizes (8 and 4) while outperforming other methods. For extremely small batch sizes (e.g. 1), we introduce DPCore-B, which uses a buffer zone to accumulate samples before updates. With a buffer size of 64, DPCore-B achieves a 41.2% error rate even with single-sample batches, demonstrating its practical utility (details in Appendix F.2).

Effect of number of source examples. We evaluate DPCore's sensitivity to source data volume by varying the number of source examples used for computing statistics from 0 to 10k. As shown in Fig. 6c, DPCore maintains effective adaptation even with 50 examples. For all main experiments, we randomly select 300 unlabeled source examples, notably different from methods like VDP, DePT, EcoTTA, and ViDA that require the entire labeled source dataset for parameter initialization. We further explore an extreme scenario where source data is completely inaccessible (shown at source data = 0 in Fig. 6c). For ImageNet-C experiments, using 300 unlabeled STL10 (Coates et al., 2011) images as reference still achieves an error rate of 45.6%, improving over the source model by 10.2%. Details are provided in Appendix F.3.

DPCore's computation and memory efficiency. We analyze computational complexity across methods in Table 10, comparing learnable parameters, forward/backward propagation counts, and relative computation time (normalized to Tent). DPCore achieves efficiency by introducing only 0.08M parameters (0.1% of model parameters), whereas ViDA requires 7.13M parameters (89× more) and 55.6% more computation time. While this analysis primarily focuses on test-time computation, DPCore also maintains efficiency in pre-adaptation: unlike previous methods which require extensive source data warm-up (e.g., EcoTTA needs 3 epochs of ImageNet training for parameter initialization), DPCore requires minimal preparation, involving only forwarding 300 source examples and computing their statistics. This shows DPCore's efficiency in both the preparation and adaptation phases. Detailed analysis is in Appendix F.4.

Table 10. Computational analysis on ImageNet-to-ImageNet-C. #Param. shows learnable parameters (Extra Param. indicates injected parameters beyond model), #FP/#BP shows propagation counts, Time shows relative computation (Tent=1.0), and Err Mean shows classification error rate (%).

Algo.	#Param.	Extra Param.	#FP	#BP	Time	Err Mean↓
Tent	0.03M		1	1	1.0	51.0
CoTTA	86.57M		11.7	1	3.6	54.8
VDP	1800	✓	2	1	1.5	50.0
EcoTTA	3.46M	✓	1	1	1.9	48.0
ViDA	93.70M	✓	11	1	2.8	43.4
Ours	**0.08M**	✓	**3.1**	**1.1**	**1.8**	**39.9**

F.2. DPCore with Small Batch Size

While DPCore performs effectively with batch sizes of four or larger (as shown in the Fig. 6d), significant challenges emerge with extremely small batches, particularly in single-sample scenarios. To address this limitation, we propose DPCore-B (DPCore with Buffer Zone), which accumulates a predefined number of samples (D) in the buffer zone before performing any updates. During this accumulation period, we temporarily store the `[CLS]` features from each batch.

Our evaluation of DPCore-B in the CSC setting with various values of D shows promising results (Table 9), effectively maintaining DPCore's performance even with small batches. However, this success is limited to the CSC setting where domain changes are structured and predictable. Even when accumulated samples span domain boundaries (violating the single-domain batch assumption shared by most CTTA methods, including ours), the impact remains minimal in CSC due to the limited number of domain transitions. For instance, on ImageNet-to-ImageNet-C with batch size 64, each domain has 782 batches, totaling 11,730 batches across 15 domains. Only 14 transition points potentially contain mixed-domain data, causing a negligible impact on overall performance.

In contrast, CDC presents a fundamentally more challenging scenario where domain transitions occur frequently and unpredictably. The substantially higher number of potential mixed-domain batches in CDC violates our method's assumptions more severely, making DPCore-B ineffective. This limitation further demonstrates why CDC, with its frequent domain changes and varying durations, better reflects real-world challenges compared to conventional CSC settings. The development of effective small-batch adaptation strategies for CDC remains an important direction for future research.

F.3. DPCore without Access to Source Data

In this section, we explore an extreme scenario where source data is completely inaccessible, further demonstrating DPCore's practicality in real-world applications. Following the insights from (Mehra et al., 2024), we propose using public datasets that share similar or identical label spaces. For instance, in ImageNet-to-ImageNet-C or CIFAR10-to-CIFAR10C tasks, we leverage STL10 (Coates et al., 2011), which shares label space with CIFAR10 despite being distinct from ImageNet.

To ensure quality reference data, we filter the public dataset using the source model with an entropy-based threshold. Specifically, following (Niu et al., 2022), we set the threshold as $0.4 \times \ln C$, where C is the number of classes in the task (e.g., 1000 for ImageNet-to-ImageNet-C). We maintain consistency with our main experiments by selecting 300 unlabeled samples from STL10 using this filtering strategy and compute statistics to replace the source statistics. Remarkably, as shown in Fig. 6c, using these 300 filtered STL10 images as reference data for ImageNet-C experiments still achieves an error rate of 45.6%, yielding a substantial 10.2% improvement over the source model. These results demonstrate that DPCore can maintain effective adaptation even without access to source data, further establishing its practical utility in real-world scenarios where source data might be unavailable due to privacy, security, or storage constraints.

F.4. Details in Computational Complexity

We provide a detailed analysis of the computation and memory efficiency of DPCore. In Table 10, we list the total number of trainable parameters required for ImageNet-to-ImageNet-C tasks. The parameter count for DPCore is not static; it increases with the addition of more core elements. The number of core elements depends on the number of unseen domains encountered. However, we demonstrate in Fig. 3c that the core set size remains stable across different domain orders of 15 corruptions in the CSC setting.

For ImageNet-to-ImageNet-C tasks, the total number of parameters is computed as the number of core elements (14) multiplied by the prompt length (8) and the dimension of each prompt token (768). The counts for forward and backward propagations are averaged per batch. In DPCore, a new prompt is learned from scratch over 50 steps only when a test batch is evaluated as originating from a potential new domain. This results in the forward and backward operations being repeated for 50 steps for these batches. Notably, only 14 prompts undergo this extensive learning process out of 11,730 batches. For the remaining batches, DPCore updates the weighted prompt in a single step (one forward and one backward operation) and then uses the updated weighted prompt to refine all existing prompts without additional forward or backward passes. Therefore, the average number of backward propagations per batch is $\frac{14\times 50+(11730-14)\times 1}{11730} \approx 1.06$. For forward propagation, each batch requires two additional forward passes (one without prompt, one with weighted prompt) for evaluation, leading to an average of $1.06 + 2 = 3.06$ forward passes.

The computational overhead of learning new prompts becomes negligible given the large number of total batches. Additionally, the parameters introduced by the prompts are minimal compared to the parameter increases required by other CTTA methods. Consequently, our prompt parameters do not require any warm-up, which conserves memory and reduces computation both before and during adaptation.

G. Limitations

While our method significantly advances CTTA, it has certain limitations that may affect its broader application. Firstly, DPCore requires access to source statistics or reference data, which may not always be available, especially in scenarios where the source data is proprietary or sensitive. Secondly, DPCore assumes that each batch of data comes from the same domain, which may not hold true in mixed-domain environments. In real-world applications, data streams could contain a mix of samples from various domains, and the method's performance in such scenarios remains to be investigated. Furthermore, while DPCore demonstrates impressive efficiency compared to other methods, it still introduces additional computational overhead during the adaptation phase, which may pose challenges in resource-constrained environments or applications with strict latency requirements.

Table 11. **Classification error rate (%) for CIFAR100-to-CIFAR100C in the CSC setting.**

Algorithm	Gauss.	Shot	Impulse	Defocus	Glass	Motion	Zoom	Snow	Frost	Fog	Bright	Contrast	Elastic	Pixel	JPEG	Mean↓	Gain↑
Source	55.0	51.5	26.9	24.0	60.5	29.0	21.4	21.1	25.0	35.2	11.8	34.8	43.2	56.0	35.9	35.4	0.0
Tent (Wang et al., 2021)	53.0	47.0	24.6	22.3	58.5	26.5	19.0	21.0	23.0	30.1	11.8	25.2	39.0	47.1	33.3	32.1	+3.3
CoTTA (Wang et al., 2022)	55.0	51.3	25.8	24.1	59.2	28.9	21.4	21.0	24.7	34.9	11.7	31.7	40.4	55.7	35.6	34.8	+0.6
VDP (Gan et al., 2023)	54.8	51.2	25.6	24.2	59.1	28.8	21.2	20.5	23.3	33.8	7.5	11.7	32.0	51.7	35.2	32.0	+3.4
ViDA (Liu et al., 2023b)	50.1	40.7	22.0	21.2	45.2	21.6	16.5	17.9	16.6	25.6	11.5	29.0	29.6	34.7	27.1	27.3	+8.1
DPCore (Proposed)	**48.2**	**40.2**	**21.3**	**20.2**	**44.1**	**21.1**	**16.2**	**18.1**	**15.2**	**22.3**	**9.4**	**13.2**	**28.6**	**32.8**	**25.5**	**25.1**	**+10.3**

Table 12. **Classification error rate (%) for CIFAR100-to-CIFAR100C in the CDC setting.**

Algorithm	Gauss.	Shot	Impulse	Defocus	Glass	Motion	Zoom	Snow	Frost	Fog	Bright	Contrast	Elastic	Pixel	JPEG	Mean↓	Gain↑
Source	55.0	51.5	26.9	24.0	60.5	29.0	21.4	21.1	25.0	35.2	11.8	34.8	43.2	56.0	35.9	35.4	0.0
Tent (Wang et al., 2021)	53.5	46.5	26.2	25.8	61.0	28.1	23.5	21.7	22.6	30.9	11.0	24.4	41.3	49.1	36.7	33.5	+1.9
CoTTA (Wang et al., 2022)	53.3	51.9	27.1	26.3	60.5	29.2	21.3	22.5	23.5	35.6	13.7	33.7	41.6	59.1	39.4	35.9	-0.5
VDP (Gan et al., 2023)	56.6	53.5	31.8	29.1	63.9	33.9	23.5	25.7	29.9	38.5	12.1	15.5	34.0	53.8	39.6	36.1	-0.7
ViDA (Liu et al., 2023b)	50.1	42.1	23.9	23.3	48.1	23.7	19.5	18.7	18.5	29.6	11.6	36.1	32.6	37.1	32.8	29.8	+5.6
DPCore (Proposed)	**54.0**	**42.5**	**23.5**	**22.8**	**45.3**	**21.4**	**18.6**	**21.2**	**16.8**	**23.2**	**10.0**	**15.1**	**35.7**	**34.6**	**25.9**	**27.4**	**+8.0**

Table 13. **mIoU score for Cityscapes-to-ACDC in the CSC setting.** The same target domains are repeated three times.

Algorithm	Round 1					Round 2					Round 3					Mean↑	Gain↑
	Fog	Night	Rain	Snow	Mean↑	Fog	Night	Rain	Snow	Mean↑	Fog	Night	Rain	Snow	Mean↑		
Source	69.1	40.3	59.7	57.8	56.7	69.1	40.3	59.7	57.8	56.7	69.1	40.3	59.7	57.8	56.7	56.7	0.0
Tent (Wang et al., 2021)	69.0	40.2	60.1	57.3	56.7	68.3	39.0	60.1	56.3	55.9	67.5	37.8	59.6	55.0	55.0	55.7	-1.0
CoTTA (Wang et al., 2022)	70.9	41.2	62.4	59.7	58.6	70.9	41.1	62.6	59.7	58.6	70.9	41.0	62.7	59.7	58.6	58.6	+1.9
DePT (Gao et al., 2022)	71.0	40.8	58.2	56.8	56.5	68.2	40.0	55.4	53.7	54.3	66.4	38.0	47.3	47.2	49.7	53.4	-3.3
VDP (Gan et al., 2023)	70.5	41.1	62.1	59.5	58.3	70.4	41.1	62.2	59.4	58.2	70.4	41.0	62.2	59.4	58.2	58.2	+1.5
SAR (Niu et al., 2023)	69.0	40.2	60.1	57.3	56.7	69.0	40.3	60.0	67.8	59.3	67.5	37.8	59.6	55.0	55.0	57.0	+0.3
EcoTTA (Song et al., 2023)	68.5	35.8	62.1	57.4	56.0	68.3	35.5	62.3	57.4	55.9	68.1	35.3	62.3	57.3	55.8	55.8	-0.9
ViDA (Liu et al., 2023b)	71.6	43.2	66.0	63.4	61.1	73.2	44.5	67.0	63.9	62.2	73.2	44.6	67.2	64.2	62.3	61.9	+5.2
C-MAE (Liu et al., 2024)	71.9	44.6	67.4	63.2	61.8	71.7	44.9	66.5	63.1	61.6	72.3	45.4	67.1	63.1	62.0	61.8	+5.1
DPCore (Proposed)	**71.7**	**47.2**	**66.1**	**63.3**	**62.1**	**73.0**	**47.8**	**66.5**	**63.1**	**62.6**	**73.4**	**47.8**	**67.1**	**62.7**	**62.8**	**62.5**	**+5.8**

Table 14. **mIoU score for Cityscapes-to-ACDC in the CDC setting.** The same target domains are repeated three times.

Algorithm	Round 1					Round 2					Round 3					Mean↑	Gain↑
	Fog	Night	Rain	Snow	Mean↑	Fog	Night	Rain	Snow	Mean↑	Fog	Night	Rain	Snow	Mean↑		
Source	69.1	40.3	59.7	57.8	56.7	69.1	40.3	59.7	57.8	56.7	69.1	40.3	59.7	57.8	56.7	56.7	0.0
Tent (Wang et al., 2021)	68.5	39.8	59.7	58.3	56.6	67.0	38.1	58.9	55.3	54.8	66.1	36.4	58.4	52.6	53.4	54.9	-1.8
CoTTA (Wang et al., 2022)	70.1	41.2	61.9	58.6	58.0	69.7	41.0	61.4	57.2	57.3	68.7	40.5	60.3	56.4	56.5	57.3	+0.5
DePT (Gan et al., 2023)	69.5	40.2	58.7	56.2	56.2	68.4	39.8	58.3	55.7	55.6	66.7	39.1	57.9	54.3	54.5	55.4	-1.3
VDP (Gan et al., 2023)	70.5	40.8	61.9	59.2	58.1	70.1	40.3	61.2	57.8	57.4	70.0	39.2	59.9	57.6	56.7	57.4	+0.7
SAR (Niu et al., 2023)	69.1	41.6	59.9	57.5	57.0	68.8	41.2	59.7	57.4	56.8	69.1	40.8	59.2	57.0	56.5	56.8	+0.1
EcoTTA (Song et al., 2023)	68.4	34.6	61.8	57.4	55.6	68.1	34.3	61.6	57.2	55.3	68.1	33.4	61.7	57.0	55.1	55.3	-1.4
ViDA (Liu et al., 2023b)	71.0	42.1	64.2	62.9	60.1	70.6	41.5	62.1	62.1	59.1	70.2	40.9	61.5	61.6	58.6	59.2	+2.5
DPCore (Proposed)	**71.9**	**46.3**	**64.1**	**63.3**	**61.4**	**71.6**	**45.1**	**63.4**	**63.1**	**60.8**	**71.6**	**44.2**	**63.9**	**63.2**	**60.7**	**61.0**	**+4.3**